Research Article

Ting Miao, Liqiong Tian, Xiaochang Leng, Zhangmu Miao, Jingjing Wang, Chengjun Xu*, Lisheng Liu

A comparative study of cohesive zone models for predicting delamination fracture behaviors of arterial wall

https://doi.org/10.1515/phys-2020-0134
received October 16, 2019; accepted April 16, 2020

Abstract: Arterial tissue delamination, manifested as the fracture failure between arterial layers, is an important process of the atherosclerotic plaque rupture, leading to potential life-threatening clinical consequences. Numerous models have been used to characterize the arterial tissue delamination fracture failure. However, only a few have investigated the effect of cohesive zone model (CZM) shapes on predicting the delamination behavior of the arterial wall. In this study, four types of CZMs (triangular, trapezoidal, linear–exponential, and exponential–linear) were investigated to compare their prediction of the arterial wall fracture failure. The Holzapfel–Gasser–Ogden (HGO) model was adopted for modeling the mechanical behavior of the aortic bulk material. The CZMs optimized during the comparison of the aortic media delamination simulations were also used to perform the comparative study of the mouse plaque delamination and human fibrous cap delamination. The results show that: (1) the numerical predicted the relationships of force–displacement in the delamination behaviors based on the triangular, trapezoidal, linear–exponential, and exponential–linear CZMs match well with the experimental measurements. (2) The traction–separation relationship results simulated by the four types of CZMs could react well as the corresponding CZM shapes. (3) The predicted load–load point displacement curves using the triangular and exponential–linear CZMs are in good agreement with the experimental data, relative to the other two shapes of CZMs. All these provide a new method combined with the factor of shape in the cohesive models to simulate the crack propagation behaviors and can capture the arterial tissue failure response well.

Keywords: cohesive zone model, fracture failure, delamination, arterial tissue, Holzapfel–Gasser–Ogden model

1 Introduction

Each year in the United States, 1.1 million people suffer from myocardial infarction with 40% fatality rate [1]. The arterial tissue fracture failure in terms of arterial wall delamination and separation is the main reason for atherosclerosis, which is likely to cause myocardial infarction [2]. There are two types of arteries: one is elastic arteries with relatively large diameters, which are located close to the heart, and the other is muscular arteries, which are distributed at the periphery. The arterial wall is composed of three layers: intima, media, and adventitia. The intima consists of a single layer of endothelial cells and a basal lamina. The media consists of a three-dimensional network of smooth muscle cells, elastin, and collagen fibers, and the adventitia consists of bundles of collagen fibers [3]. It is known that elastin is the major load-bearing components of the arterial wall at low strain and that collagen fibers contribute to the stiffening of the arterial tissue at high strain as they are gradually recruited [4]. The structure of the arterial tissue specifically accounts for the distinct mechanical behaviors that the stress–strain curve shows a lower load response at the stage with larger displacement applied and a sharp increase in load with limit displacement. The mechanical

* **Corresponding author: Chengjun Xu,** School of Logistics Engineering, Wuhan University of Technology, Wuhan 430063, China, e-mail: chengjunxu1973@163.com
Ting Miao: School of Transportation, Wuhan University of Technology, Wuhan 430063, China; School of Urban Construction, Wuchang University of Technology, Wuhan 430223, China
Liqiong Tian: PowerChina Jiangxi Electric Power Engineering CO., LTD, Nanchang, China
Xiaochang Leng: School of Civil Engineering and Architecture, Nanchang University, Nanchang, China
Zhangmu Miao: School of Transportation, Wuhan University of Technology, Wuhan 430063, China
Jingjing Wang: Department of Cardiology, Chinese PLA General Hospital, First Medical Center, Beijing 100853, China
Lisheng Liu: School of Urban Construction, Wuchang University of Technology, Wuhan 430223, China

properties of each layer of the arterial wall depend on its composition and microstructure and the mechanical properties of the primary load-bearing components. Hypertension or trauma may induce geometrical mismatch and interlayered shear stress concentration between layers [5,6]. Moreover, intra-layer dissection of the arterial wall in terms of split and cleavage usually occurs in the media [7,8]. With the dissections inside the medial layer, blood will bulge the delaminated medial layer, reducing the lumen of the blood vessel and compromising the strength of the arterial wall. Therefore, there is a pressing need to investigate the mechanism of the dissection at the medial layer.

Numerous experimental studies focused on the evaluation of the arterial medial layer dissection. Sommer et al. [8] investigated the dissection of human abdominal medial layers via peeling tests and quantified the dissection energy. Tong et al. [9] studied the dissection properties and mechanical strength of the carotid artery and found that interfacial ruptures mainly occurred at the media. Thus, the study on the delamination behaviors of the arterial wall, especially in the medial layer, is of great importance.

Cohesive zone model (CZM) approach has been used to model the medial layer dissection. Gasser and Holzapfel [10] implemented the CZM to model the arterial layer dissection and showed that the obtained gap-displacement vs load/width curves were in good agreement with the experimental measurements [8]. Ferrara and Pandolfi [4] utilized an anisotropic CZM in the numerical simulation to investigate the interlamellar tearing in the media [8] and captured the main response of the arterial tissue fracture failure.

It has been shown that the triangular CZM and the exponential CZM are usually used in the simulations, playing an important role in the traction–separation behavior at the delamination crack front during the tearing propagation, especially for metal and composite materials [11–13]. The results of these works demonstrate that the ductile behavior or softening behavior of the materials can affect the strength predictions of the CZM. Moreover, the mechanical response of the arterial tissue is largely governed by the orientation and mechanical properties of collagen fibers during the crack initiation and propagation, giving an exponential increase in the stress–strain relationships of the arterial wall. However, few studies have investigated the effect of CZM shapes on the delamination fracture behavior of the arterial tissue.

This study focuses on the comparison of four different shapes (triangular, trapezoidal, linear–exponential, and exponential–linear) of CZM in modeling the arterial medial layer peeling. Meanwhile, as a continuation of the previous studies, four types of CZM laws are used to model the delamination fracture of atherosclerotic plaque and fibrous cap [14,15]. The findings of this study will help to study the influence of cohesive law shapes on the tearing propagation behavior in the medial layer of the arterial tissue. To be more specific, simulating the arterial tissue dissection to predict the delamination behaviors of the arterial wall promotes the development of effective techniques for performing the treatment and intervention.

2 Materials and methods

In this study, the Holzapfel–Gasser–Ogden (HGO) model [16] was used to characterize the anisotropic hyperelastic mechanical behavior of the arterial tissue. Four types of CZMs (triangular, trapezoidal, linear–exponential, and exponential–linear) were used to simulate the delamination behavior along the medial interface of the arterial wall.

2.1 Bulk material model: HGO model

Free energy, Ψ, the potential energy per unit volume of arterial material defined in decoupled form, is expressed as follows:

$$\Psi = \Psi_{\text{vol}} + \bar{\Psi}. \tag{1}$$

The volumetric part, Ψ_{vol}, is given, according to Gasser et al. [16], as follows:

$$\Psi_{\text{vol}} = \frac{1}{D}\left(\frac{J^2 - 1}{2} - \ln J\right), \tag{2}$$

where $\frac{1}{D}$ approximates to the bulk modulus of the material, and $J = \det(F)$, where F is the deformation gradient.

The isochoric potential is given as follows:

$$\bar{\Psi} = \bar{\Psi}_{\text{g}} + \bar{\Psi}_{\text{f}}, \tag{3}$$

which is composed of two parts. One is used to describe the mechanical response of the matrix:

$$\bar{\Psi}_{\text{g}} = \frac{\mu}{2}(\bar{I}_1 - 3). \tag{4}$$

Another is implemented to represent the mechanical behavior of the two families of collagen fibers:

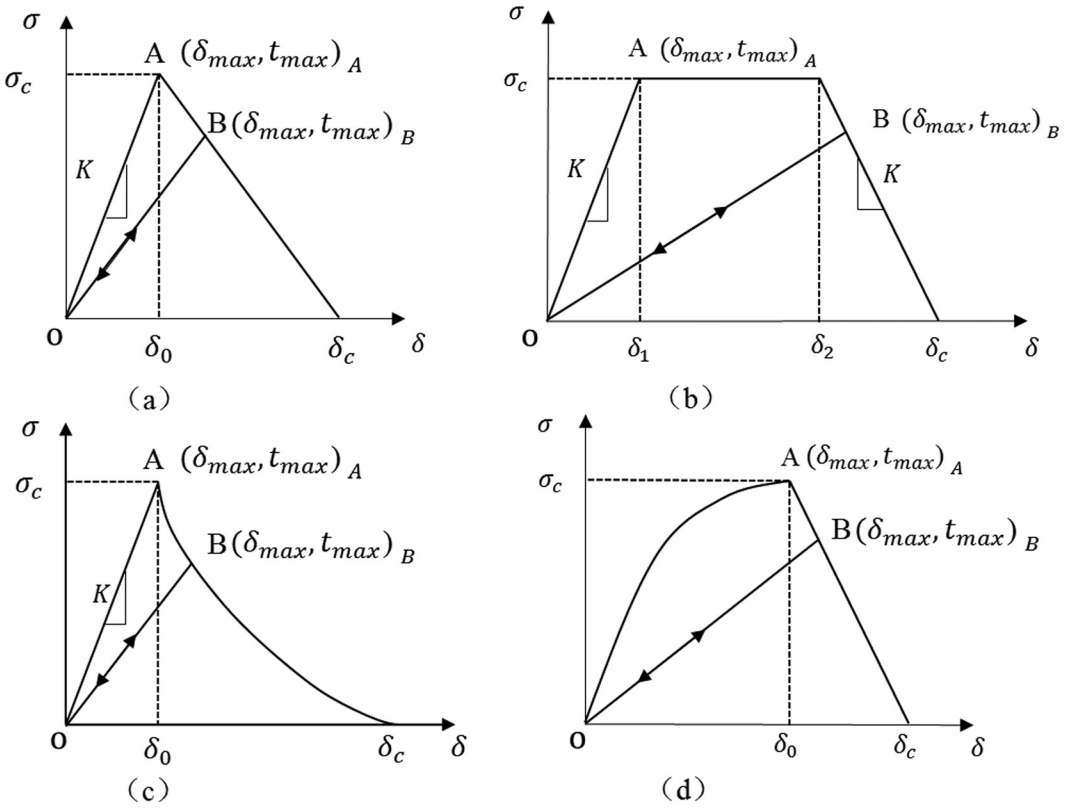

Figure 1: Four types of irreversible cohesive model denoted with effective traction and displacement: (a) triangular CZM, (b) trapezoidal CZM, (c) linear–exponential CZM, and (d) exponential–linear CZM.

$$\bar{\Psi}_{\mathrm{f}}(\bar{\boldsymbol{C}}, \boldsymbol{H}_1, \boldsymbol{H}_2) = \frac{k_1}{2k_2}\left[\mathrm{e}^{k_2[\kappa\bar{I}_1+(1-3\kappa)\bar{I}_{41}-1]^2} - 1\right] + \frac{k_1}{2k_2}\left[\mathrm{e}^{k_2[\kappa\bar{I}_1+(1-3\kappa)\bar{I}_{42}-1]^2} - 1\right], \tag{5}$$

where $\bar{I}_1 = \mathrm{tr}(\bar{\boldsymbol{C}})$ denotes the first invariant of $\bar{\boldsymbol{C}}$ and μ is the neo-Hookean parameter, which characterizes the shear modulus of the material without fibers; $\bar{I}_{41} = \boldsymbol{a}_{01}\cdot\bar{\boldsymbol{C}}\boldsymbol{a}_{01}$ and $\bar{I}_{42} = \boldsymbol{a}_{02}\cdot\bar{\boldsymbol{C}}\boldsymbol{a}_{02}$ are the tensor invariants, which are equal to the square of the stretch in the directions of $[\boldsymbol{a}_{01}] = [\cos\gamma, \sin\gamma, 0]$ and $[\boldsymbol{a}_{02}] = [\cos\gamma, -\sin\gamma, 0]$, respectively. Note that the constitutive parameter k_1 is related to the relative stiffness of the fibers, which is determined from the mechanical tests of tissue, and k_2 is the dimensionless stiffness. As described in reference [17], the parameter κ is the dispersion parameter, which characterizes the dispersion of the two families of fibers along the two average distributed directions, and $0 \le \kappa \le 1/3$, when $\kappa = 0$, each family of collagen fibers is parallel to each other, and when $\kappa = 1/3$, the random distribution of the fibers is equivalent to an isotropic material. γ represents the angle between the mean fiber orientation of one family of fibers and the circumferential direction of the aorta [18].

2.2 Interfacial CZM

Four types of CZMs are implemented in this study through a user-defined subroutine UEL in ABAQUS [19]. With the CZM parameter, which characterizes the relationship between the cohesive force of the interface and the separation force of the interface, the "effective" opening displacement δ is given by:

$$\delta = \sqrt{\lambda^2\delta_{\mathrm{s}}^2 + \delta_{\mathrm{n}}^2}, \tag{6}$$

where λ is a scalar parameter being introduced to assign different weights to the opening displacement δ_{n} and the sliding displacement δ_{s}. The parameter δ_{s} is denoted by:

$$\delta_{\mathrm{s}} = \sqrt{\delta_{\mathrm{s1}}^2 + \delta_{\mathrm{s2}}^2}, \tag{7}$$

where δ_{s1} and δ_{s2} represent the components of the two directions of the sliding displacement δ_{s} passing through the cohesive surfaces.

According to the theory of CZM, the delamination fracture failure of arterial layers contains three steps.

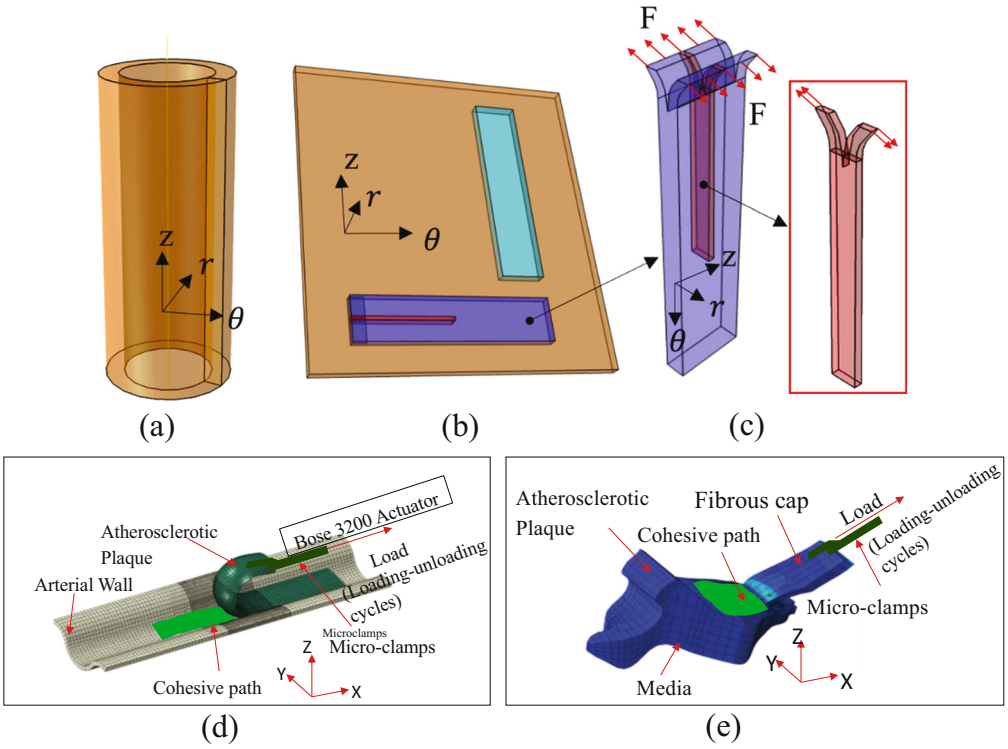

Figure 2: A schematic of the arterial layer peeling test setup. (a) A part of aorta; (b) a flat of arterial layer after cutting from (a); (c) an arterial strip, which was peeled at one end, and the geometric model of the peeling test for the simulation (in the red line box); (d) the simulation predicted load–load point displacement curves of the mouse atherosclerotic plaque delamination; and (e) the simulation predicted load–load point displacement curves of the human fibrous cap delamination under loading–delamination–unloading cycles.

The first step is damage initiation. When the "effective" opening displacement reaches δ_0 (for triangular, linear–exponential, and exponential–linear CZMs; Figure 1) or δ_1 (for trapezoidal CZM; Figure 1), the cohesive elements start to degrade. Meanwhile, the effective traction t (Cauchy stress) reaches the cohesive strength σ_c of the interface. The expressions of effective traction t and the first-order partial derivative of the effective traction t to the effective opening displacement – $\frac{\partial t}{\partial \delta}$ are given in chapter 3 of reference [17] (Appendix A). The second step is damage evolution. In this step, the accumulation of damage occurs in the cohesive element. The damage variable d is introduced to quantitatively evaluate the damage. Evidently, d ranges from 0 to 1, representing the cohesive surfaces without damage and the complete separation of the cohesive surfaces, respectively. The loading and unloading processes of the cohesive traction–separation criterion are illustrated in Figure 1. When the effective traction t exceeds σ_c, the damage accumulates, as the point A reflects in Figure 1. When the curves unloaded at points A and B, respectively, permanent damage occurs at the cohesive surfaces at points A and B. Therefore, the traction–separation relationship curve will travel along the lines AO and BO. Conversely, when no damage occurs on the cohesive surface, the traction–separation curve will follow the original curve. The third step is that the cohesive elements completely failed after the effective displacement reaches the critical effective separation value δ_c (as shown in Figure 1). Meanwhile, the critical energy release rate G_c is attained. All the expressions for the four types of CZMs can be found in chapter 3 of reference [17] (Appendix A).

2.3 Arterial tissue delamination

Three different arterial tissue delamination experiments were performed in different research studies to find the mechanism of arterial tissue failure. With regard to the media delamination processes, the geometrical model is reconstructed based on the experiments of the peeling test of human aortic media [8] (Figure 2a–c). The geometrical dimensions of the arterial wall are 4 mm of length, 1.2 mm of width, and 0.05 mm of thickness. For the mouse plaque delamination test (Figure 2d), an exposed aorta was fastened to a small plate connected to the load cell for load data recording and sequential loading–delamination–unloading cycles were applied to cause the plaque delaminating from the underlying arterial tissue [14]. For the human fibrous cap

delamination test, as shown in Figure 2e, the delamination of human fibrous cap presents as a pair of micro–clamps. The sequential loading–delamination–unloading cycles are applied to make the fibrous cap separate from the underlying plaque tissue [15]. Although there are three types of delamination experiments, the HGO models and CZM models used for the simulation are the same, except for the human aortic media delamination test (including viscoelastic material model parameters for human arterial tissue) and the material parameter values for the three cases.

3 Numerical implementations

3.1 Arterial wall delamination modeling using CZMs

In this section, to predict the delamination fracture behaviors of the arterial tissue, a part of the arterial wall is utilized to perform experiment and simulation. The sampling method for the experiment is shown in Figure 2. The geometrical model is reconstructed based on the experiments of the peeling test of human aortic media [8], as shown in the red box of Figure 2c. The geometrical dimensions of the arterial wall are 4 mm of length, 1.2 mm of width, and 0.05 mm of thickness. The front and back surfaces of the strip (Figure 2c, in the red line box) are fixed along the z direction for the sake of computational efficiency. The delamination behavior is modeled as plane strain deformation.

To evaluate the performance of the arterial wall dissection, the finite element (FE) simulations are implemented using ABAQUS [19–21], associated with a user-defined subroutine modeling the delamination fracture of the cohesive interface in the arterial layer. The arterial layer is meshed with 1920 eight-node hexahedral elements, C3D8H, where the cohesive interface is meshed with 72 zero-thick eight-node 3D user-defined elements. A layer of cohesive elements is placed along the mode I delamination (crack growth) path starting from the initial peeling front to the end of arterial strip (Figure 2c). The size of the elements for the FE model is 0.05 mm, based on the parametric analysis. Presetting the peeling path can increase the computational efficiency of the CZM model in the practice of simulating interface material separation events. The peeling path is obtained from the experimental observations of this study. Meanwhile, the experimental setup and simulation modeling details of the mouse plaque delamination and human fibrous cap delamination processes are presented in references [14,15].

3.2 Parameter selection in modeling

The parameter values for the HGO and CZM models were taken from references [4,10,22]. The value of the interfacial stiffness K was assigned as the same one from reference [14]. With regard to the simulations of the mouse plaque delamination processes, the material parameter values for the HGO and CZM models were adopted from reference [14] and those values of the human fibrous cap delamination were obtained from reference [15] (including viscoelastic material model parameters for human arterial tissue), as shown in Table 1.

3.3 Results of simulations and experiments

The parameters used for the simulations of the arterial layer peeling test (Figure 2) are set with the same values as shown in Table 1. The pulling forces divided by the width of the specimen vs the load point displacement are shown in Figure 3. The pulling forces per unit of width are between 25.5 and 28.5 mN/mm, which are in the domain of the experimental results (23–35 mN/mm) [8].

The deformed configurations of the aortic media delamination are shown in Figure 4a. The contour levels shown in the figure represent the normal component of the Cauchy stress to the delamination plane. U is defined as the load point displacement (five stages). The traction–separation (displacement) relationships in terms of a cohesive element in the middle of the crack path are presented in Figure 4b.

The load–load point displacement curves are shown in Figures 5a and 6a. The traction separation (displacement) relationships of a cohesive element in the middle of the crack growth path for the plaque and the fibrous cap are shown in Figures 5b and 6b.

4 Results comparison and discussion

The aim of this study is to compare the four different shapes (triangular, trapezoidal, linear–exponential, and exponential–linear) of the CZM in modeling the arterial medial layer peeling (Figures 3 and 4). Moreover, four types of CZM laws were used to model the delamination of atherosclerotic plaque [14] (Figure 5) and fibrous cap [15] (Figure 6).

Table 1: Material parameter values for arterial layer and CZM parameter values for cohesive layer

Arterial media peeling [10,4,22]	HGO model	μ (MPa)	k_1 (MPa)	k_2	γ (deg.)	κ		
		0.0162	0.0981	10	5	0		
	CZM	G_c (N/mm)	σ_c (MPa)	K (N/mm^3)	λ			
		0.049	0.14	1×10^3	10			
Mouse plaque delamination [14]	HGO model	μ (MPa)	k_1 (MPa)	k_2	γ (deg.)	κ		
	Media	0.004	4	525	46.4	0.226		
	Plaque	0.004	4	525	27.2	0.226		
	CZM	G_c (N/mm)	σ_c (MPa)	K (N/mm^3)	λ			
		0.019	0.14	1×10^4	1.2			
Human fibrous cap delamination [15]	HGO model	μ (MPa)	k_1 (MPa)	k_2	γ (deg.)	κ	T_1 (s)	β_1
	Media	0.0014	0.206	58.55	28.35	0.29	5.8	10
	Plaque	0.04945	0.0237	2,630	30	0.226	2.06	20
	Fibrous cap	0.02189	0.09363	7,957	17.22	0.226	—	—
	CZM	G_c (N/mm)	σ_c (MPa)	K (N/mm^3)	λ			
		0.23	0.42	1×10	1			

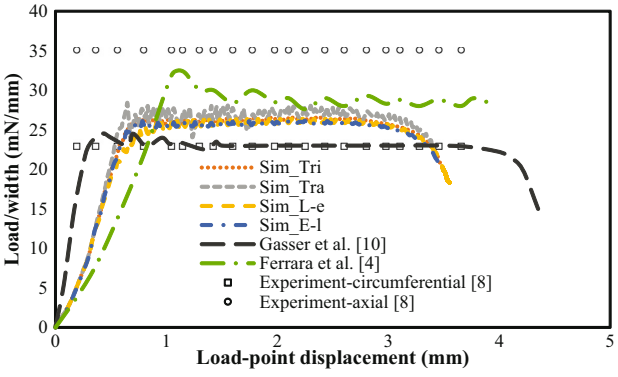

Figure 3: Comparison of the load/width–load point displacement curves between the simulation and average experimental results.

4.1 Aortic media delamination

The comparison of the four shapes of CZM laws for modeling the aortic media delamination was described in terms of the load/width–load point displacement curves, tensile stress contour, and traction–displacement curves. This study simulated the aortic media delamination experiments in Sommer et al. [8] by four types of CZMs and further compares the results with the simulations in Gasser and Holzapfel [10] and Ferrara and Pandolfi [4]. Figure 3 shows that some research records in this study are within the range of the known results of the previous studies. The pulling forces per unit of width (load/width) are between 25.5 and 28.5 mN/mm, which are in good agreement with the numerical results by Gasser and Holzapfel (23 mN/mm)

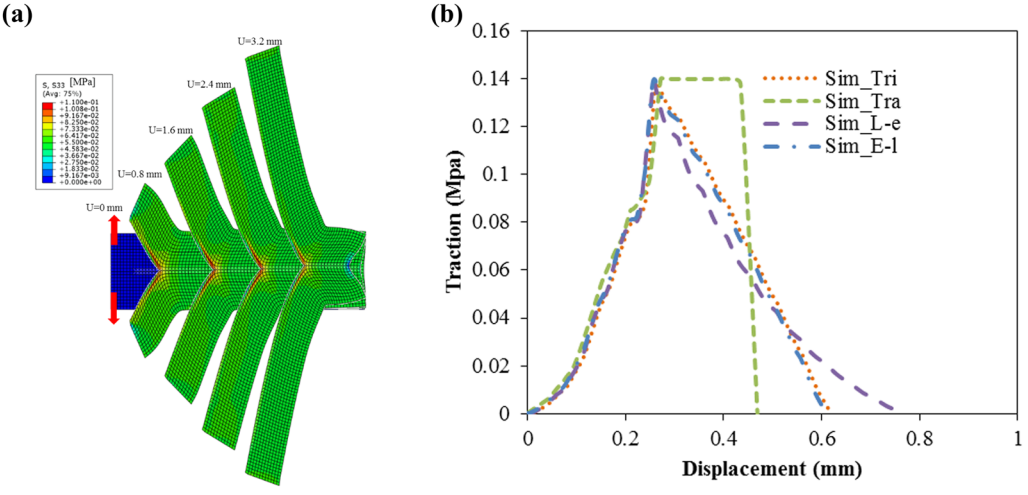

Figure 4: (a) Tensile stress contour of the arterial wall at five levels of the aortic media peeling. (b) The traction–separation (displacement) relationship of a cohesive element in the middle of the crack path.

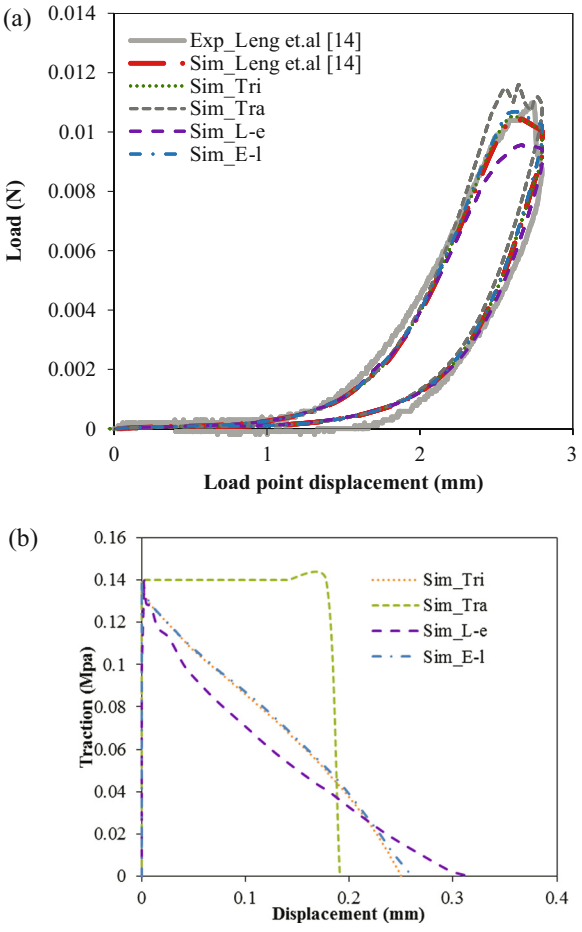

Figure 5: (a) The simulation predicted load–load point displacement curves of the mouse atherosclerotic plaque delamination are compared with the experimental measured curves. (b) The traction–separation curves of a cohesive element in the middle of the crack path.

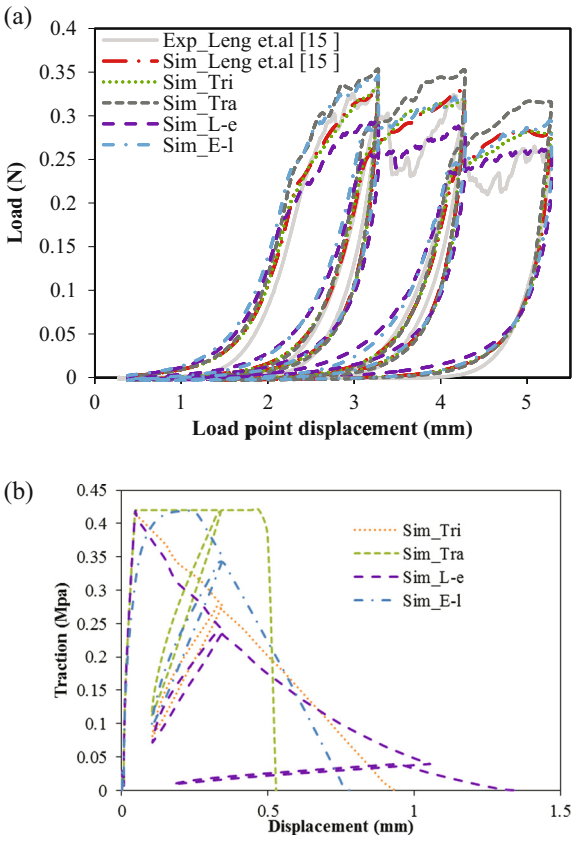

Figure 6: (a) The simulation predicted load–load point displacement curves of the human fibrous cap delamination under loading–delamination–unloading cycles are compared with the experimental measured curves. (b) The traction–separation curves of a cohesive element in the middle of the crack path.

[10] and Ferrara and Pandolfi (28.8 mN/mm) [4]. Also, the CZM simulation of peeling load/width ratio is in the range of 22.9–34.8 mN/mm, which is based on the peeling tests of the rectangular-shaped medial strips along the circumferential and axial directions by Sommer et al. [8]. For the traction–separation relationships, it is observed that the shape of the softening stage (after the initial damage) is almost the same as the shape of the corresponding CZM, as shown in Figure 4b.

4.2 Mouse plaque delamination and human fibrous cap delamination

Besides, the comparison of the results of the experiment of the aortic media delamination and the simulation of mouse plaque delamination [14] and human fibrous cap delamination [15] was carried out to compare with the simulation results obtained using four types of CZMs. A mesh dependency study of the mouse plaque and human fibrous cap delamination was conducted in the previous works [14,15,23], in which the selected mesh refinement is enough to obtain the convergence solutions. For these two delamination simulations, the magnitude of the maximal force during delamination predicted by the linear–exponential CZM is lower by nearly 10%, while the magnitude predicted by the trapezoidal CZM is higher by nearly 4% than that reported in the previous studies [14,15,24] (Figures 5a and 6a). The load–load point displacement curves of other two types of CZMs (triangular and exponential–linear) match well with the experiments and simulations of the previous studies [14,15]. The minimum values of the traction (linear–exponential CZM) compared with the other shapes of the CZMs reveal that the reaction forces (Figures 5a and 6a) during the plaque and fibrous cap delamination are less than the other types of the CZMs. Figures 5b and 6c show the traction–separation relationships in four types of CZMs; the traction of the

elastic stage of the CZM for the plaque delamination rapidly increases to the maximum value (Figure 5b). For the fibrous cap delamination, the tractions of the elastic stage of the CZMs are similar to the shapes of the CZMs (Figure 6b). For both delamination, it shows that the shapes of the softening stage are almost the same as the shapes of the corresponding CZMs. The unloading and loading processes of the element under unloading and loading cycles are shown in Figure 6b, indicating that the softening of the element experiences a long loading displacement.

4.3 Effects and features of four shapes of CZMs in simulating the delamination behaviors

The shapes of the traction–separation curves of an element at the front of the crack are in good agreement with the shape of CZM laws used to simulate the aortic delamination process (Figure 4b), showing that the extent of damage evolution is the largest for the linear–exponential CZM, followed by the triangular, exponential–linear, and trapezoidal CZM laws. However, this respective order does not represent the order of the predicted load/width values (Figure 3). The trapezoidal law shows higher values of transmission of the load/width at the initial stage of damage, because the maximum traction kept constant under the longest displacement load during the damage evolution process compared with the other shapes of CZM laws. The triangular CZM can obtain the predicted load/width or load with an acceptable accuracy, and it is the easiest CZM law to use in terms of simulation of the arterial tissue fracture failure. At the stage when a cohesive element is totally failed, the release area of the bulk material will induce a contraction, which indicates that the oscillation for the predicted load using the trapezoidal CZM is more obvious than that by other CZM laws.

The iterative process and the time for acquiring the solutions are influenced by the shape of CZM laws. The degree of difficulty to get convergence solutions in the iterative process is the highest for the trapezoidal, followed by the linear–exponential, exponential–linear, and triangular CZMs.

The elastic deformation of the cohesive element is governed by the mechanical properties of its structural constituents and the interfacial strength of the material (e.g., triangular and trapezoidal CZM). The nonlinearity of the traction–separation relationship of the cohesive element is largely attributed to the gradual recruitment of the load-bearing collagen fibers with increasing pressures [25–27]. The softening of the traction–separation relationship is attributed to the softening behavior of the medial interfacial strength, plaque, or fibrous cap [28–30]. Hence, these CZMs are able to characterize the mechanical response of the cohesive element during the crack propagation.

5 Conclusion and discussion

In this work, the studies on the delamination fracture behaviors of the arterial tissue have been conducted, combined with the CZM numerical simulation and experiments. The main observations have been pointed out as follows.

Frist, four types of CZMs (triangular, trapezoidal, linear–exponential, and exponential–linear) have been used to simulate the aortic media peeling. The investigated results indicate that the prediction of the load–load point displacement curves, which is based on the CZMs, matches well with the experimental measurements of the aortic media peeling process.

Second, the simulation of the arterial wall delamination, which is based on the four types of CZMs, indicated that the simulation results of the traction–separation relationships could react well as the corresponding CZM shapes.

Third, to investigate the effect of CZM shapes on the failure strength predictions, the comparative study of numerical predictions for the mouse plaque and human fibrous cap delamination events is also conducted based on the four CZMs, which reflect the actual crack growth well during the simulation of the aortic media delamination events. The results demonstrate that the triangular and exponential–linear CZMs match well with the experimental force–displacement curves, while the trapezoidal CZM overpredicts and the linear–exponential CZM underpredicts the force during the load–load point displacement relationships.

Fourth, in terms of the study on the effects and features of the four shapes of CZMs above, the results indicate that the four shapes of CZMs have their own advantage in simulating the delamination behaviors. All these provide a new method combined with the factor of shape in the cohesive models to simulate the crack propagation behaviors.

The limitations of this study are related to the referenced assumptions. The fiber-reinforced constitutive model takes into account the changes in the orientation of collagen fibers. However, the previous studies [31,32] have demonstrated a continuous distribution of fiber orientations. Furthermore, the proposed layered constitutive model assumes that the composition and structure of the arterial wall are uniform in the radial direction. A more detailed assessment of the composition and structure of the arterial

wall results in a more accurate numerical prediction of the arterial tissue failure.

Acknowledgment: Research reported in this publication was supported by the National Natural Science Foundation Youth Fund of China (No. 11802113).

References

[1] Lekoubou A, Ovbiagele B, Markovic D, Sanossian N, Towfighi A. Age, sex, and race/ethnic temporal trends in metabolic syndrome prevalence among individuals with myocardial infarction or stroke in the United States. J Neurological Sci. 2017;376:24–8.
[2] Wang Y, Ning JF, Johnson JA, Sutton MA, Lessner SM. Development of a quantitative mechanical test of atherosclerotic plaque stability. J Biomech. 2011;44(13):2439–45.
[3] Holzapfel GA, Gasser TC, Ogden RW. A new constitutive framework for arterial wall mechanics and a comparative study of material models. J Elast Phys Sci Solids. 2000;61:1–48.
[4] Ferrara A, Pandolfi A. A numerical study of arterial media dissection processes. Int J Fract. 2010;166:21–33.
[5] Badel P, Avril S, Sutton MA, Lessner SM. Numerical simulation of arterial dissection during balloon angioplasty of atherosclerotic coronary arteries. J Biomech. 2014;47(4):878–89.
[6] Wang Y, Johnson JA, Fulp A, Sutton MA, Lessner SM. Adhesive strength of atherosclerotic plaque in a mouse model depends on local collagen content and elastin fragmentation. J Biomech. 2013;46(4):716–22.
[7] Gasser TC, Holzapfel G. Modeling Plaque Fissuring and Dissection during Balloon Angioplasty Intervention. Ann Biomed Eng. 2007;35(5):711–23.
[8] Sommer G, Gasser TC, Regitnig P, Auer M, Holzapfel GA. Dissection properties of the human aortic media: an experimental study. J Biomechancial Eng. 2008;130(2):021007.
[9] Tong J, Sommer G, Regitnig P, Holzapfel G. Dissection properties and mechanical strength of tissue components in human carotid bifurcations. Ann Biomed Eng. 2011;39(6):1703–19.
[10] Gasser TC, Holzapfel GA. Modeling the propagation of arterial dissection. Eur J Mech - A/Solids. 2006;25(4):617–33.
[11] Camanho PP, Davila C, De Moura M. Numerical simulation of mixed-mode progressive delamination in composite materials. J Composite Mater. 2003;37(16):1415–38.
[12] Roychowdhury S, Arun Roy YD, Dodds Jr RH. Ductile tearing in thin aluminum panels: experiments and analyses using large-displacement, 3-D surface cohesive elements. Eng Fract Mech. 2002;69(8):983–1002.
[13] Prim DA, Zhou B, Hartstone-Rose A, Uline MJ, Shazly T, Eberth JF. A mechanical argument for the differential performance of coronary artery grafts. J Mech Behav Biomed Mater. 2016;54:93–105.
[14] Leng X, Chen X, Deng X, Sutton MA, Lessner SM. Modeling of experimental atherosclerotic plaque delamination. Ann Biomed Eng. 2015;43(12):2838–51.
[15] Leng X, Davis LA, Deng X, Sutton MA, Lessner SM. Numerical modeling of experimental human fibrous cap delamination. J Mech Behav Biomed Mater. 2016;59:322–36.
[16] Gasser TC, Ogden RW, Holzapfel GA. Hyperelastic modelling of arterial layers with distributed collagen fibre orientations. J R Soc, Interface/R Society. 2006;3(6):15–35.
[17] Leng X. Numerical studies of arterial tissue failure. PhD Dissertation. University of South Carolina; 2016.
[18] Leng X, Zhou B, Deng X, Davis L, Lessner SM, MA, Sutton, et al. Experimental and numerical studies of two arterial wall delamination modes. J Mech Behav Biomed Mater. 2017;77:321–30.
[19] ABAQUS. Analysis user's manual version 6.12. Dassault Systemes Corp; 2013.
[20] Shazly T, Rachev A, Lessner S, Argraves WS, Ferdous J, Zhou B, et al. On the uniaxial ring test of tissue engineered constructs. Exp Mech. 2015;55(1):41–51.
[21] Zhou B, Sit AJ, Zhang X. Noninvasive measurement of wave speed of porcine cornea in ex vivo porcine eyes for various intraocular pressures. Ultrasonics. 2017;81:86–92.
[22] Zhou B, Alshareef M, Prim D, Collins M, Kempner M, Hartstone-Rose A, et al. The perivascular environment along the vertebral artery governs segment-specific structural and mechanical properties. Acta Biomaterialia. 2016;45:286–95.
[23] Zhou B, Wolf L, Rachev A, Shazly T. A structure-motivated model of the passive mechanical response of the primary porcine renal artery. J Mech Med Biol. 2014;14(03):1450033.
[24] Zhang X, Osborn T, Zhou B, Meixner D, Kinnick R, Bartholmai B, et al. Lung ultrasound surface wave elastography: a pilot clinical study. IEEE Trans Ultrason Ferroelectr Freq Control. 2017;64(9):1298–304.
[25] Zhou B, Rachev A, Shazly T. The biaxial active mechanical properties of the porcine primary renal artery. J Mech Behav Biomed Mater. 2015;48:28–37.
[26] Twal WO, Klatt SC, Harikrishnan K, Gerges E, Cooley MA, Trusk TC, et al. Cellularized microcarriers as adhesive building blocks for fabrication of tubular tissue constructs. Ann Biomed Eng. 2014;42(7):1470–81.
[27] John TS, Eberth F, Boran Z, Prim DA. Conrad Michael Gore. Pulsatile perfusion bioreactor for mimicking, controlling, optimizing blood vessel mech. US Pat. 15/071,354, 2016.
[28] Kalra S, Osborn T, Bartholmai B, Zhou B, Zhang X. Lung ultrasound surface wave elastography-preliminary measurements in patients with interstitial lung diseases, respirology. vol. 22, 111 River St, Hoboken 07030-5774, NJ USA: Wiley; 2017. p. 90.
[29] Zhou BDA, Prim, E, Romito, McNamara LP, Spinale FG, Shazly T, et al. Contractile smooth muscle and active stress generation in porcine common carotids. J Biomech Eng. 2017;140:1.
[30] Kubo K, Zhou B, Cheng Y, Yang T, Qiang B, An K, et al. Ultrasound elastography for carpal tunnel pressure measurement: a cadaveric validation study. J Orthopaedic Res. 2017;36(1):477–83.
[31] Zhang X, Osborn T, Zhou B, Bartholmai B, Greenleaf JF, Kalra S. An ultrasound surface wave elastography technique for noninvasive measurement of surface lung tissue. J Acoustical Soc Am. 2017;5:3721.
[32] Campillho RDSG, Banea MD, Neto JABP, da Silva LFM. Modelling adhesive joints with cohesive models: effect of the cohesive law shape of the adhesive layer. Int J Adhes Adhesives. 2013;44:48–56.

Appendix A [17]

Triangular CZM

A triangular form of energy release rate for the cohesive surface can be expressed as follows:

$$G_c = \frac{1}{2}\sigma_c \delta_c. \tag{A1}$$

The displacement jump for the damage initiation and complete damage of the cohesive element is denoted by:

$$\delta_0 = \frac{\sigma_c}{K}, \tag{A2}$$

$$\delta_c = \frac{2G_c}{\sigma_c}, \tag{A3}$$

where K is the penalty stiffness.

The effective traction can be expressed as follows:

$$t = \begin{cases} \dfrac{\delta}{\delta_0}\sigma_c\,, & \delta \le \delta_0 \\ \sigma_c\left(\dfrac{\delta_c - \delta}{\delta_c - \delta_0}\right) = \sigma_c(1-d)\,, & \delta_0 \le \delta < \delta_c \\ 0\,, & \delta_c \le \delta. \end{cases} \tag{A4}$$

The first-order partial derivative of the effective traction t with respective to the effective opening displacement is given by:

$$\frac{\partial t}{\partial \delta} = \begin{cases} \dfrac{\sigma_c}{\delta_0}\,, & \delta \le \delta_0 \\ \dfrac{-\sigma_c}{\delta_c - \delta_0} = \dfrac{-\sigma_c d}{\delta - \delta_0}, & \delta_0 \le \delta < \delta_c \\ 0\,, & \delta_c \le \delta\,, \end{cases} \tag{A5}$$

where d is the damage variable defined to represent the softening of the cohesive element:

$$d = \begin{cases} 0, & \delta \le \delta_0 \\ \dfrac{G_c - \left[\sigma_c\left(\frac{\delta_c - \delta}{\delta_c - \delta_0}\right)\delta_c\frac{1}{2}\right]}{G_c} = \dfrac{\delta - \delta_0}{\delta_c - \delta_0}, & \delta_0 \le \delta < \delta_c \\ 1\,, & \delta_c \le \delta. \end{cases} \tag{A6}$$

Trapezoidal CZM

A trapezoidal form of energy release rate for the cohesive surface can be expressed as follows:

$$G_c = \frac{1}{2}\sigma_c[(\delta_2 - \delta_1) + \delta_c]. \tag{A7}$$

The displacement jump for the damage initiation, traction softening initiation, and complete damage of the cohesive element is denoted by:

$$\delta_1 = \frac{\sigma_c}{K}, \tag{A8}$$

$$\delta_2 = \frac{G_c}{\sigma_c}, \tag{A9}$$

$$\delta_c = \delta_1 + \delta_2, \tag{A10}$$

where K is the penalty stiffness.

The effective traction can be expressed as follows:

$$t = \frac{\partial \varphi}{\partial \delta} = \begin{cases} \dfrac{\delta}{\delta_1}\sigma_c, & \delta \le \delta_1 \\ \sigma_c, & \delta_1 \le \delta < \delta_2 \\ \dfrac{(1-d)(\delta_2 - \delta_1 + \delta_c)}{\delta_c}\sigma_c, & \delta_2 \le \delta < \delta_c \\ 0, & \delta_c \le \delta. \end{cases} \tag{A11}$$

The first-order partial derivative of the effective traction t with respective to the effective opening displacement is given by:

$$\frac{\partial t}{\partial \delta} = \begin{cases} \dfrac{\sigma_c}{\delta_1}, & \delta \le \delta_1 \\ 0, & \delta_1 \le \delta < \delta_2 \\ -\sigma_c\dfrac{(1-d)(\delta_2 - \delta_1 + \delta_c)}{\delta_c(\delta_c - \delta)}\,, & \delta_2 \le \delta < \delta_c \\ 0, & \delta_c \le \delta \end{cases} \tag{A12}$$

where d is the damage variable defined to represent the softening of the cohesive element:

$$d = \begin{cases} 0, & \delta \le \delta_1 \\ \dfrac{(\delta - \delta_1)}{(\delta_2 - \delta_1 + \delta_c)}, & \delta_1 \le \delta < \delta_2 \\ 1 - \dfrac{\delta_c(\delta_c - \delta)}{(\delta_c - \delta_2)(\delta_2 - \delta_1 + \delta_c)}, & \delta_2 \le \delta < \delta_c \\ 1, & \delta_c \le \delta \end{cases}. \tag{A13}$$

Linear–exponential CZM

A linear–exponential form of energy release rate for the cohesive surface can be expressed as follows:

$$G_c = \sigma_c(\delta_c - \delta_0)\left(1 - \frac{1}{1 - e^{-\alpha}} + \frac{1}{\alpha}\right), \tag{A14}$$

where α is the shape of the exponential law ($\alpha = 2$).

The displacement jump for the damage initiation and complete damage of the cohesive element is denoted by:

$$\delta_0 = \frac{\sigma_c}{K} \tag{A15}$$

$$\delta_c = \frac{G_c}{\sigma_c\left(1 - \frac{1}{1 - e^{-\alpha}} + \frac{1}{\alpha}\right)} + \delta_0, \tag{A16}$$

where K is the penalty stiffness.

The effective traction can be expressed as follows:

$$t = \begin{cases} K\delta, & \delta \le \delta_0 \\ K\delta(1 - d), & \delta_0 \le \delta < \delta_c \\ 0, & \delta_c \le \delta. \end{cases} \tag{A17}$$

The first-order partial derivative of the effective traction t with respective to the effective opening displacement is given by:

$$\frac{\partial t}{\partial \delta} = \begin{cases} K, & \delta \le \delta_0 \\ (1 - d)K, & \delta_0 \le \delta < \delta_c \\ 0, & \delta_c \le \delta, \end{cases} \tag{A18}$$

where d is the damage variable defined to represent the softening of the cohesive element:

$$d = \begin{cases} 0, & \delta \le \delta_0 \\ 1 - \dfrac{\delta_0}{\delta_{\max}}\left[1 - \dfrac{1 - \exp\left[-\alpha\left(\frac{\delta_{\max} - \delta_0}{\delta_c - \delta_0}\right)\right]}{1 - \exp(-\alpha)}\right], & \delta_0 \le \delta < \delta_c \\ 1, & \delta_c \le \delta. \end{cases} \tag{A19}$$

Exponential–linear CZM

A triangular form of energy release rate for the cohesive surface can be expressed as follows:

$$G_c = \frac{\sigma_c}{K}\left[K\delta_0 - \sigma_c + \sigma_c \exp\left(-\frac{\delta_0 K}{\sigma_c}\right)\right] + \frac{1}{2}\sigma_c(\delta_c - \delta_0). \tag{A20}$$

The displacement jump for the damage initiation and complete damage of the cohesive element is denoted by:

$$\delta_0 = -\frac{\ln(e)\sigma_c}{K} \tag{A21}$$

$$\delta_c = \frac{2G_c}{\sigma_c} - \frac{2}{K}\left[K\delta_0 - \sigma_c + \sigma_c \exp\left(-\frac{\delta_0 K}{\sigma_c}\right)\right] + \delta_0, \tag{A22}$$

where K is the penalty stiffness.

The effective traction can be expressed as follows:

$$t = \begin{cases} \sigma_c\left(1 - \exp\left(-\dfrac{\delta K}{\sigma_c}\right)\right), & \delta \le \delta_0 \\ (1 - d)(1 - e)\sigma_c\dfrac{\delta}{\delta_0}, & \delta_0 \le \delta < \delta_c \\ 0, & \delta_c \le \delta. \end{cases} \tag{A23}$$

The first-order partial derivative of the effective traction t with respective to the effective opening displacement is given by:

$$\frac{\partial t}{\partial \delta} = \begin{cases} K\exp\left(-\dfrac{\delta K}{\sigma_c}\right), & \delta \le \delta_0 \\ (1 - d)(1 - e)\dfrac{\sigma_c}{\delta_0}, & \delta_0 \le \delta < \delta_c \\ 0, & \delta_c \le \delta, \end{cases} \tag{A24}$$

where d is the damage variable defined to represent the softening of the cohesive element:

$$d = \begin{cases} 0, & \delta \le \delta_0 \\ 1 - \dfrac{\delta_0(\delta_c - \delta_{\max})}{\delta_{\max}(\delta_c - \delta_0)}, & \delta_0 \le \delta < \delta_c \\ 1, & \delta_c \le \delta. \end{cases} \tag{A25}$$